Biochimica et Biophysica Acta 806 (1985) 93–106
Elsevier

BBA 41682

Picosecond studies at 77 K of energy transfer in chloroplasts at low and high excitation intensities

Bruce Wittmershaus [a], Thomas M. Nordlund [a,*], Wayne H. Knox [b,¶], Robert S. Knox [a], Nicholas E. Geacintov [c] and Jacques Breton [c,d]

[a] *Department of Physics and Astronomy, and* [b] *Institute of Optics and Laboratory for Laser Energetics, University of Rochester, Rochester, NY 14627,* [c] *Chemistry Department, New York University, New York, NY 10003 (U.S.A.) and* [d] *Dépertement de Biologie, Centre d'Etudes Nucleaires de Saclay, 91191 Gif-sur-Yvette Cedex (France)*

(Received May 23rd, 1984)
(Revised manuscript received September 26th, 1984)

Key words: Energy transfer; Chlorophyll fluorescence; (Spinach chloroplast)

Spinach chloroplast chlorophyll fluorescence at 685 and 735 nm (F_{685} and F_{735}) has been time-resolved with a low-jitter streak camera system. Measurements are reported largely for 77 K, using single 30-ps 532-nm excitation pulses with pulse fluences of $2 \cdot 10^{12}$ to $2 \cdot 10^{16}$ photons $\cdot$ cm^{-2}. A slightly fluence-dependent delay (16 ± 3 ps) found for the rise of F_{735} relative to F_{685} is too small to correspond to transfer into the species emitting F_{735} from the species emitting F_{685}. The rise of F_{735} is biphasic at lower intensities and monophasic at higher intensity. The delay in the rise of F_{685} is smaller than approx. 2 ps. The time-resolved F_{685} is fit with a three-component model in which energy is transferred from a large pool of antenna chlorophylls to a small pool closely connected to the reaction center, all exciton annihilation occurring in the small pool. The F_{735} biphasic rise and its sensitivity to excitation fluence is explained by a similar but independent model. Data at our lowest intensities are consistent with those obtained by a photon-counting method using very low intensity excitation.

Introduction

Time-resolved fluorescence data have been used for over 10 years as an indicator of the locus of relaxed electronic excitation energy in algae, chloroplasts, and subchloroplast particles [1]. The primary feature in early picosecond pulse data obtained was an anomalously short intrinsic fluorescence lifetime. Exciton annihilation, as suggested by several authors [2–4], was shown to be the cause of most of the systematically shortened fluorescence traces [5]. This effect was subsequently used to study excitation diffusion in spinach chloroplasts and the topology of the photosynthetic unit [6,7]. Another line of investigation, using photon-counting methods (see, for instance, Refs. 8–10), has employed excitation intensities sufficiently low that nonlinear effects are virtually certain to be absent.

Time-dependent fluorescence meaurements obtained at high excitation intensities have been erratic even when the nonlinear effects have been recognized explicitly and taken into account in the analyses. In Fig. 1 we show a selection of time parameters measured subsequent to pulse excita-

* Also now at: Department of Radiation Biology and Biophysics, School of Medicine and Dentistry, University of Rochester, Rochester, NY 14642, U.S.A.
¶ Present address: ATT Bell Laboratories, Holmdel, NJ 07733, U.S.A.

Abbreviations: LHC, light-harvesting chlorophyll; PS I, II, Photosystem I, II; OMA, optical multi-channel analyzer.

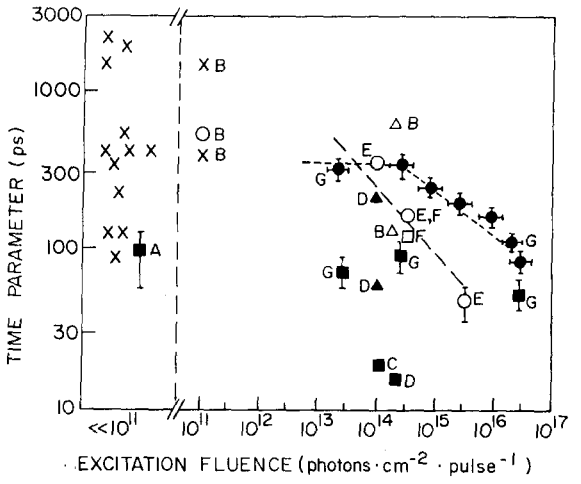

Fig. 1. Selected fluorescence response parameters in various species and under various conditions, as a function of excitation pulse intensity. Symbols: circles (○, ●) represent 1/e-decay times of F_{685} and squares (□, ■) represent 10–90% rise-times of F_{735}; the other symbols (×, ▲, △) each represent the lifetime parameter in one component of a multiexponential fit to spinach chloroplasts (●, ■, ▲), *Chlorella* (○, □), wild-type barley chloroplasts (△). The points marked × refer to various species. The dashed lines merely aid the eye in correlating the data in two sets of measurements (E and G) and have no particular quantitative significance. Error bars represent ranges quoted in references, and in case G the spread consistent with kinetic fits (vertical direction) or an estimated 10% error in energy determination (horizontal direction). References: A, Reisberg et al. [17]; B, Beddard et al. [12]; C, Pellegrino et al. [14]; D, Yu et al. [16]; E, Campillo et al. [4]; F, Campillo et al. [13]; G, present work. Most data shown here are representative of 77–90 K, with some at 300 K (case B) and in the case of D no appreciable temperature dependence occurred.

tion to illustrate this point [4,9–17]. Probably the data scatter problem is caused partially by the use of widely varying conditions, species and instrumentation, partially by details of interpretation, and partially by signal-to-noise limits in measurements involving streak cameras. The last is largely responsible for the lack of measurements in the 10^{11}–10^{13} fluence range. In the range below 10^{11}, there are three clusters of data points, one around 100 ps, one around 450 ps. and another around 2000 ps. These represent the lifetimes used in fitting linear combinations of exponentials to 685 nm fluorescence. Reisberg et al. [17] believe that as many as three different lifetime components are ultimately nescessary for this type of analysis of the fluorescence around 685 nm. Another feature of Fig. 1 is the spread of the data on 735 nm rise-times (the square points). This will be discussed in the Experimental results and the Analysis sections.

Although the fluorescence of chloroplasts at 77 K originates in a variety of emitters [18], two wavelength regions have dominated high-intensity research. F_{685}, around 685 nm, can be regarded loosely as the fluorescence from light-harvesting chlorophyll (LHC), and from chlorophyll antenna molecules associated primarily but not exclusively with System II (PS II). F_{735}, around 735 nm, originated in System I (PS I). F_{685} has a rise which follows the 532 nm excitation as faithfully as if the excitation were directly into the emitting states (less than 2 ps delay time). F_{735} has a 10–90% rise-time (reported variously from 20 to 150 ps) usually attributed to the time of energy transfer to a species called C-705 [19]. As the excitation intensity increases, the 1/e decay time of F_{685} decreases. That of the F_{735} has not been seen to decrease. The fluorescence yield of both emissions drops off at high intensities [20]. Fluorescence at 695 nm (F_{695}) is associated with System II (PS II), but because of its complexity, time-resolved measurements have not been analyzed in detail [17].

The purpose of the present investigations has been to make studies of the type just described with special attention to reproducibility and with a physical approach to the fitting of the data. The next section describes the materials and methods followed by a section in which the experimental results are described which are in the form of 685 and 735 nm fluorescence intensities as a function of time after pulse excitation. The fourth section is an analysis of the results in terms of the several possible kinetic schemes. The final section contains a summary and comments on proposed extensions of the work.

Materials and Methods

1. Sample preparation

Spinach leaves were obtained from a local supermarket. Chloroplasts were prepared following the procedure of Breton et al. [21] in a buffer solution of 0.4 M sucrose, 20 mM KCl, and 20 mM Tris buffer with no Mg^{2+} added (pH 8 at 4°C). Final solutions at 65–70% glycerol buffer

were prepared to an absorbance of up to 0.15 at 532 nm, to ensure uniform sample excitation. Samples were kept dark and on ice until use. Chloroplast suspensions were placed in a glass cuvette of path-length 1 or 0.5 mm. Each sample was mounted on a copper sample holder attached to the cold finger of a closed cycle helium refrigerator system (CTI-Cryogenics). To minimize the creation of freezing cracks, the samples were cooled rapidly to 220 K and then slowly by 20-K intervals to 80 K. From room temperature to 200 K the samples were kept under constant illumination (0.1 W/cm^2 in the 520–540 nm region) to insure that the reaction centers of Photosystem II were frozen into their closed state. Once in the range 77–80 K, the samples were maintained to within 1 K by the cryogenic system.

2. Excitation pulses and fluorescence detection

We excited the samples with single, 30-ps, 532-nm laser pulses from a frequency-doubled active-passive mode-locked Nd:YAG (neodymium^{3+}: yttrium aluminum garnet) laser system [21] at a repetition rate of about 0.5 Hz. A Schott 2 mm BG18 filter (Schott Optical Glass) was placed after the doubling crystal to block any remaining 1064 nm laser light. Schott glass neutral-density filters were used to control the incident pulse energy. To insure excitation by the pulse only, a 530 nm interference filter was placed over the sample chamber entrance window. At low intensities a cylindrical lens was used to create a spatially narrow incident pulse to permit maximum time resolution. To obtain high intensities a spherical lens was used. The angle between the incident beam and the normal to the sample surface was approx. 30°. The average energy of the excitation pulses was measured with an Rj-7200 Energy Ratiometer (Laser Precision Corporation). The single-pulse fluence of the 532 nm excitation ranged from $2 \cdot 10^{12}$ to $2 \cdot 10^{16}$ photons $\cdot$ cm^{-2} per pulse. The sample was masked to maximize the spatial uniformity of the excitation intensity and to minimize collection of fluorescence not from the primary excitation region. Nonuniformity is a special problem when nonlinear effects are under study [23].

F_{685} and F_{735} were measured independently by placing, respectively, a 14-nm-bandwidth, 685-nm interference filter and a 30-nm-bandwidth 735-nm interference filter (Pomfret Research Optics) before the streak camera collection lens. In addition, cutoff filters (Schott RG-645 and RG-715, respectively) were used to eliminate scattered 532-nm radiation and unwanted fluorescence. Time profiles for the incident 532 nm pulses were obtained by measuring the 532 nm light scattered from the sample.

Fluorescence was collected at 90° to the excitation and imaged with an $f/1.9$ achromatic lens on the photocathode of a streak-camera tube which was driven with a solid-state deflection circuit [24] (see Fig. 2). This system allows for simple addition of many single-shot measurements for signal averaging with relative time-axis deviations (jitter) of less than approx. 2 ps. Typically 100–400 shots were summed.

The image generated by the streak camera was amplified by a four-stage magnetically focused intensifier (EMI) and then imaged onto a silicon-intensified target (SIT) vidicon detector which is read by an optical multi-channel analyzer system, OMA-II (Model 1216 detector controller and Model 1215 system processor, EG&G Princeton Applied Research). The amount of background noise accumulated was reduced by gating the vidicon detector using a high voltage pulser (Model 1211, EG&G Princeton Applied Research).

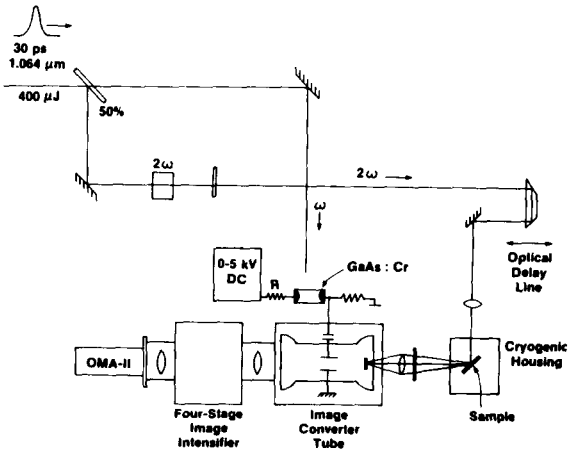

Fig. 2. Schematic of the low-jitter, signal-averaging streak camera. The photoconductive switch synchronizes the image-converter-tube ramp with the arrival of the excitation pulse at the sample [24].

The detection system gain was adjusted to yield the best signal-to-noise for the lowest level of excitation and remained at these settings for all measurements. The wide range of excitation level required the use of neutral density filters to attenuate the fluorescence collected at the higher excitation fluences to prevent the signal from saturating the system. This is why the signal-to-noise ratio of the data presented does not increase dramatically as the excitation level increases.

The focused spatial image diameter varies less than one OMA channel in the range 530–735 nm. This diameter and the time per OMA channel for the data presented were, respectively, 12 channels and 1.226 ps per channel for Figs. 4–7 and 14 channels and 0.947 ps per channel for Fig. 3. There were 470 OMA channels used to detect the time-dispersed fluorescence image generated by the streak camera.

3. Data acquisition and analysis

We operate the OMA-II in 'open system', which allows the implementation of custom data acquisition and reduction routines. In particular, an alternate background subtraction routine has been implemented [25] in which the instrument background (which originates mostly in the SIT-vidicon tube) is subtracted out immediately after each laser firing. This method effectively cancels the long-term instrumental background drift caused by temperature fluctuations in the detector array and allows detailed meaurements of very small signals (yield, approx. 10^{-6}) which are a small fraction of the instrumental background level.

The data presented in this paper have been corrected for nonlinearity in the system's response to signal intensity and non-uniformity in the channel-to-channel response in the detector. The time axis is calibrated using the multiple reflections of a 30 ps, 532 nm pulse from a 125 ps etalon [26]. The deviation from the average number of OMA channels per 125 ps interval is not more than 15% and typically not more than 5% during the first three quarters of a full scan. All corrections and fittings were performed on the OMA-II or another LSI-11 based computer work station.

Experimental results

1. Connection with photon-counting results

Since early streak-camera research involved high fluences, well above 10^{13} units *, there was concern that exciton annihilation and other nonlinear effects would compete with physiologically interesting decay mechanisms and render fluorescence interpretation difficult. A number of laboratories thus began to use photon counting techniques with excitation fluences in the 10^{6}–10^{11} range. The temporal resolution of present photon counting systems is limited by their impulse response widths, at best about 150–200 ps [17], as compared with 1 to 2 ps resolution in a streak camera. Deconvolution techniques in photon counting allow determination of lifetimes as short as 25 ps under optimal conditions [26].

Reisberg et al. [17] analyzed their photon-counted F_{685} of spinach chloroplasts at 77 K in terms of a linear combination of three exponentials. We have measured F_{685} under excitation fluences as low as $2 \cdot 10^{12}$ units, which from a physiological viewpoint can still be regarded as 'very high intensity', but the spinach chloroplast appears to respond in a linear fashion. To show this we might simply compare the data of Ref. 17 with ours, but our excitation pulses and system responses were different. We have therefore taken the three-exponential linear combination of Ref. 17 as the true delta function response of the fluorescing system and convolved it with our pulse. This is the smooth solid line in Fig. 3, along with a curve typical of F_{685} at an excitation fluence of $2.2 \cdot 10^{13}$ units. The excellent agreement of these curves demonstrated linear response to our satisfaction. The fluorescence yield has also been found to remain constant up through similar intensities [20].

Photon-counting curves and our streak-camera curves are in reasonably good agreement for the rising phase of the 735 nm fluorescence, also, but only if the lower limiting values of the exponential-fitting lifetime parameters of Ref. 17 are used. In Fig. 3, the long and medium components are

* In this section all fluences will be stated in units of photons per cm^2 per pulse. Note that intensities are in units of fluence per unit time.

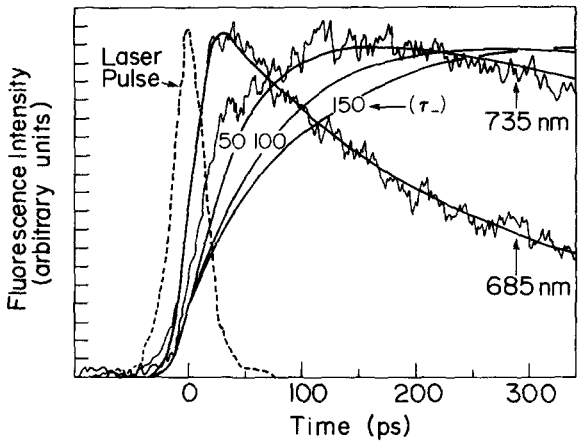

Fig. 3. F_{685} and F_{735} from 77 K spinach chloroplasts at an excitation fluence of $2.2 \cdot 10^{13}$ photons per cm^2; 200 shots averaged per curve. The excitation pulse (dashed curve) is measured by time-resolving the 532 nm light scattered by the sample. The smooth curves are the simulated responses to a gaussian excitation pulse of 30 ps FWHM (full width at half-maximum), using the deconvolution parameters of Reisberg et al. [17] for a comparison of photon-counting and streak camera results. These parameters are for F_{685} $\alpha_1 = 13$, $\tau_1 = 1520$ ps; $\alpha_2 = 49$, $\tau_2 = 320$ ps; $\alpha_3 = 38$, $\tau_3 = 140$ ps and for F_{735} are $\alpha_1 = 46$, $\tau_1 = 2200$ ps, $\alpha_2 = 10$, $\tau_2 = 400$ ps, $\alpha_- = -44$, and $\tau_- = 100 \pm 50$ ps, where α_i is the relative amplitude of the ith deconvoluted decay component and τ_i is the respective lifetime. For this and all theoretical curves in subsequent figures, a gaussian pulse modelled directly after the measured excitation pulse is used as the excitation profile in kinetic equations.

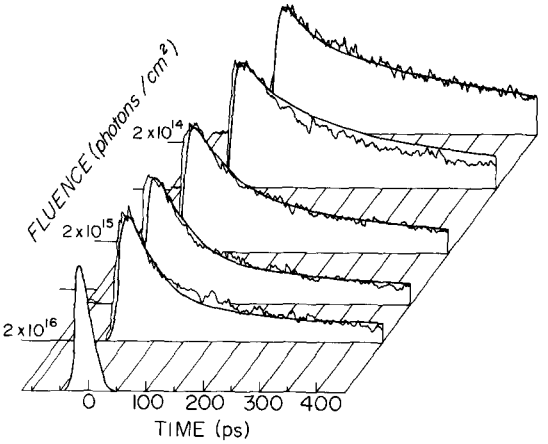

Fig. 4. Time-resolved F_{685} form 77 K spinach chloroplasts and its dependence on excitation fluence (units: photons per cm^2 per pulse). Experimental curves are normalized and in arbitrary units. Fluences and the number of shots averaged are $1.6 \cdot 10^{14}$ (200 shots), $5.6 \cdot 10^{14}$ (100 shots), $2.6 \cdot 10^{15}$ (100 shots), $8.2 \cdot 10^{15}$ (100 shots) and $2.0 \cdot 10^{16}$ (100 shots). The smooth curves are theoretical fits generated by summing the three components of the coupled model (see Fig. 9b and Table I).

fixed at 2200 and 400 ps, respectively, for all three smooth curves. Whereas Reisberg et al. quote a range of 50–150 ps for the short component, only the 50 ps limit is consistent with our data. Holding this constant and relaxing the long component to 3000 ps removes the agreement in the range above 300 ps. We can make the distinction among short-time components because of our greater timing precision, but we cannot make strong statements about the long-time component because of the limited time duration of our measurements.

2. Intensity dependence of fluorescence decay

2A. F_{685}. Fig. 4 shows the time-course of F_{685} under a sequence of fluences, $1.6 \cdot 10^{14}$ through $2.0 \cdot 10^{16}$ units. Results obtained at $2.4 \cdot 10^{12}$ units are identical to those observed at $2.2 \cdot 10^{13}$ units (Fig. 3), within the noise of the measurement. We can facilitate a quantitative description of these results by referring to the simplest equation for exciton annihilation kinetics [28,29]:

$$\frac{dn}{dt} = I\sigma_0 n_0 - \beta n - \gamma n^2 \qquad (1)$$

in which n is an excitation density, I the excitation light density, σ_0 the ground-state absorption cross-section, n_0 the density of chromophores being excited, β a first-order decay constant, and γ the biomolecular decay or 'annihilation' constant. Eqn. 1 is easily solved in the steady state or under delta-function excitation or by integrating numerically for a given $I(t)$. The fluorescence of the system is proportional to $\beta_0 n(t)$, where β_0 is the natural radiation rate. In the steady-state case, Eqn. 1 leads to the well-known fluorescence yield result [29]:

$$\phi_F(I_a) = \phi_0 \frac{\beta}{I_a} \ln\left(1 + \frac{I_a \gamma}{\beta}\right) \qquad (2)$$

were ϕ_0 is the low-fluence yield (β_0/β) and I_a is the integrated absorption $\int I\sigma_0 n_0 dt$.

An important characteristic of the fluorescence data of Fig. 4 is that it cannot be fit to the solution of Eqn. 1. It is possible to force fit any one curve

with a single β and γ, but different values would be needed at different intensities. The resolution of this problem is that more than one decay component appears in the data. This is consistent with the known heterogeneity of 77 K chloroplast fluorescence (see subsection 3B, p. 99).

It is also clear that Eqn. 2, being based on single-component kinetics, cannot be a completely meaningful basis for understanding the chloroplast fluorescence yield (e.g., Ref. 30) unless one component dominates.

2B. F_{735}. Fig 5 contains F_{735} data at six fluences ranging from $4.9 \cdot 10^{13}$ to $2.0 \cdot 10^{16}$ units. In the range of $4.9 \cdot 10^{13}$ down to $2.4 \cdot 10^{12}$ units, no appreciable change in the fluorescence time profile could be seen within the noise of the measurement. There is a noticeable change in apparent lifetime under the higher excitation. It has been generally held [1] that intrinsic exciton annihilation processes do not affect the 735 nm emitting pool, but this belief was based on experiments reaching fluence of only $2.6 \cdot 10^{15}$ units [20]. Theoretical curves shown as smooth solid lines in Fig. 5 are based on the model of the Analysis section. The annihilation constant required for these curves is one or two orders of magnitude smaller than is the typical of antenna chlorophyll aggregates in vivo [1].

3. Intensity dependence of fluorescence rise-times

3A. F_{685}. The long-term stability of the solid-state deflection circuit used here enables time-axis registrations of fluorescence traces to an accuracy (approx. 1 ps) much smaller than the pulse width. In the 3-year series of measurements reported here, we have never observed a delay due to transfer processes occurring between excitation at 532 nm and emission at 685 nm. The F_{685} rise-time is characteristic of a directly excited emitter displaying rapid intermolecular relaxation. If indirect excitation via energy transfer occurs, it does so within 2 ps, or it contributes a relatively small amount to the fluorescence observed. This result is consistent with and tends to strengthen the known limit of the intramolecular chlorophyll *a* relaxation time (less than 10 ps [31]) under similar conditions.

There is an intensity dependence of the rise-curves which must be due to a nonlinear effect. One possibility is ground-state depletion ('saturation'). However, we have generally found in kinetic fitting that this is a small effect, since there is usually a small percentage of chlorophylls excited

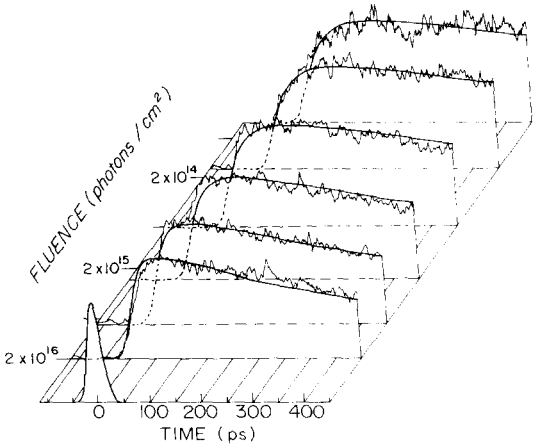

Fig. 5. Time-resolved F_{735} from 77 K spinach chloroplasts and its dependence on excitation fluence (units: photons per cm^2 per pulse). Experimental curves are normalized and in arbitrary units. Fluences and the number of shots averaged are $4.9 \cdot 10^{13}$ (400 shots), $1.6 \cdot 10^{14}$ (200 shots), $6.9 \cdot 10^{14}$ (100 shots), $2.6 \cdot 10^{15}$ (100 shots), $8.2 \cdot 10^{15}$ (100 shots) and $2.0 \cdot 10^{16}$ (100 shots). The theoretical fits shown are the time-courses of the third component (only) of the model defined by Fig. 9d, and the parameters in Table I.

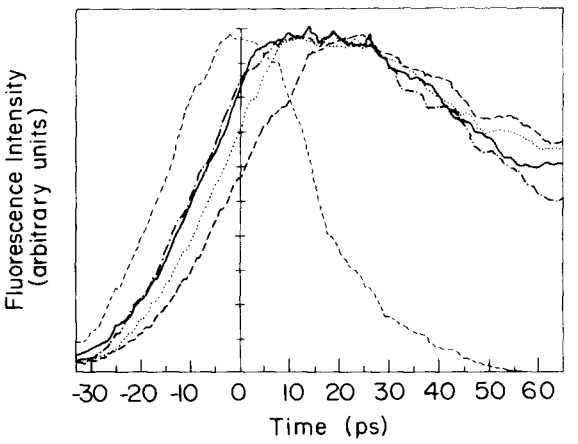

Fig. 6. High-time-resolution F_{685} dependence on excitation fluence (units: photons per cm^2 per pulse), at 77 K. The intrinsic rise-time is less than 2 ps, the resolution of the system. The measured excitation pulse is shown as the more symmetric dashed curve (------). Fluences are $5.6 \cdot 10^{14}$ (– – – –), $2.6 \cdot 10^{15}$ (· · · · · ·), $8.2 \cdot 10^{15}$ (———) and $2.0 \cdot 10^{16}$ units (· – · – ·). One OMA channel equals 1.226 ps.

even at high intensities. Another possibility is 'lifetime reduction' by exciton annihilation, which better describes the intensity dependence seen in Fig. 6.

3B. F_{735}. Fig. 7 shows the rise of F_{735} on an expanded scale. The behavior is different from that of F_{685} in two major respects. First, there is a delay, seen as a shift, of 16 ± 3 ps from the corresponding half-maximum of F_{685}. This is manifested in a 10–90% rise-time of 90 ± 10 ps at lower intensities, which drops to 55 ± 10 ps at high intensity. Such a small observed rise-time cannot be related simply to a rate constant because the pulse must be deconvolved and the kinetics considered (see the Analysis section). Second, there is a change from biphasic to monophasic rise with increasing excitation fluence (Fig. 5). The second phase of the rise can be seen setting in at $t = 25$ ps in Figs. 7 and 3.

The F_{735} risetime is observed to vary most widely in previous experiments (Fig. 1; [13,14,17 and 32]). With the exception of the data from the CUNY group [14,16] (and in a weaker sense that of Butler et al. [32]) all previous 735 nm rise-times are in the range of 50–150 ps. The main differences in Refs. 14 and 16 are the higher temperature (at least 90 K) and use of a shorter pulse (6 ps). Neither of these would seem likely to explain the discrepancy, but a temperature dependence of the rise sufficient to do so would be very interesting. With respect to the 50–150 ps range, the tendency in our data for a biphasic rise, disappearing at high intensities, helps explain why workers with lower time resolution and varying intensities could disagree widely. A further complication is the known heterogeneity of 'F_{735}' [33–36]. Our biphasic rise is in agreement with certain details of the data of Campillo et al [13] which have been neither appreciated nor reexamined since their appearance.

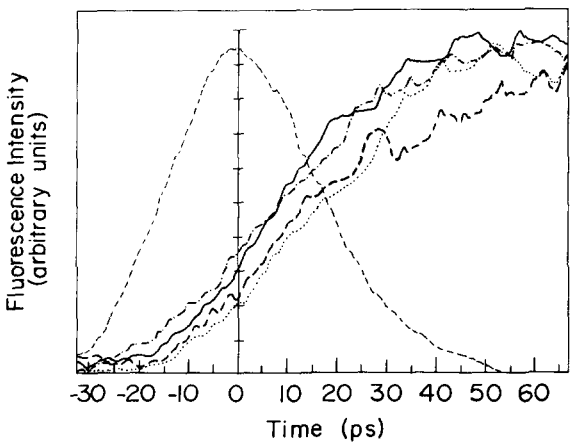

Fig. 7. Same as Fig. 6, except with emission at 735 nm. Fluences are $1.6 \cdot 10^{14}$ (– – – –), $6.9 \cdot 10^{14}$ (· · · · · ·), $2.6 \cdot 10^{15}$ (————), and $2.0 \cdot 10^{16}$ units (· – · – ·).

4. Remarks

The time-resolved data presented are representative of our measurements. Three of at least twenty sample data sets were discarded because of gross differences from published data [13,17] and from our typical results. Our steady-state 77 K chloroplast fluorescence spectra are similar to other measurements [37,48] and we have seen some minor variability in the relative peak heights of F_{685}, F_{695} and F_{735}, possibly due to seasonal changes [37]. Such variations could affect our measured decay profiles for F_{685} which contain a significant contribution from F_{695}. This may explain our few inconsistent data sets but, since a majority of our results are characterized by a single set of curves, slight variations in steady-state emission apparently have minor effects on our time-resolved fluorescence measurements.

Analysis

1. Background

An earlier analysis of time-resolved chloroplast fluorescence by Campillo et al. [13] was made semiquantitatively with the two-component model shown in Fig. 8a. The elements LH1, LH2 and PS II were treated as a single species emitting at 685 nm. The equations appropriate to low-intensity excitation on this model are:

$$\frac{dn_{II}}{dt} = G(t) - (K + \beta_{II}) n_{II}$$

$$\frac{dn_{I}}{dt} = K n_{II}(t) - \beta_{I} n_{I}$$

where n refers to excitation density and $G(t)$ is a source function. Campillo et al. were able to interpret their data with the constants $\beta_I = (1.5 \text{ ns})^{-1}$, $K = (140 \text{ ps})^{-1}$, and an intensity-dependent value for $(\beta_{II} + K)$ of $(900 \text{ ps})^{-1}$ at low fluences and of

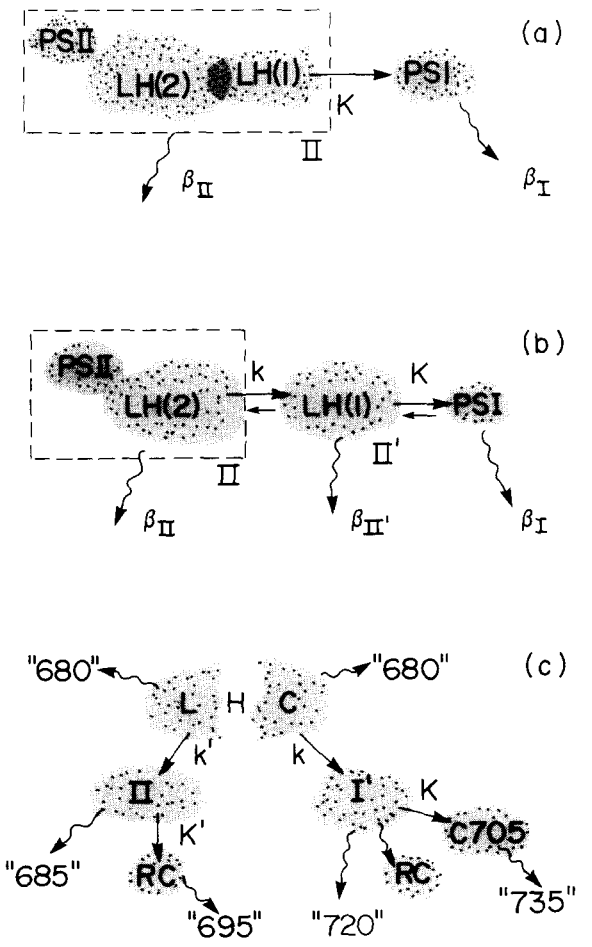

Fig. 8. (a) and (b) Elementary two-part and three-part models proposed earlier [13] and used for semiquantitative analysis of chloroplast fluorescence. The decay rates refer to fluorescence, while k and K are excitation transfer rate constants. Back-transfer paths are not labelled and are discussed in the text, as are other aspects of the diagrams. (c) A composite kinetic model forming the basis of separate fits to the 685-nm and 735-nm fluorescence data. Numbers in quote marks represent peak wavelenghts of hypothesized component fluorescence bands. As subsequently used, the rate constants K and k' are large, of the order $(20\ \text{ps})^{-1}$, while k is moderate, of the order $(200\ \text{ps})^{-1}$, and K' is as yet unspecified but helps determine the decay of 'II'.

$(139\ \text{ps})^{-1}$ at higher fluences $(2 \cdot 10^{14}$ units). Variability in β_{II} was interpreted as due to annihilation effects. The value of K^{-1} given by these authors was quoted as the 10–90% rise-time of F_{735}. The actual value of K, as obtained by fitting the solution for $n_i(t)$ to the observed rise-time, is $(37\ \text{ps})^{-1}$.

Campillo et al. considered the different rates observed for the decay of n_{II} (F_{685}) and the rise of n_I (F_{735}) as evidence that a two-component model was inadequate for describing their data. They proposed but did not work out the predictions of the three-part model of Fig. 8b, in which the existence of two rates, k and K, were to handle the dual-rate problem. Part II′ of the model would have low fluorescence yield because of the rapid transfer to part I.

Although very little theoretical work has been devoted to explaining picosecond time-resolved fluorescence data in photosynthesis [38], yields as a function of picosecond pulse intensity have received a great deal of theoretical attention [6,7, 32,39–41]. With remarkably few model assumptions it has been possible to deduce sizes of photosynthetic domains (regions over which excitation diffuses). The theories employed do not predict time dependences because they involve probabilities, not rates; and when time does enter, averages are taken quite early in the theory.

The formalism we employ is capable of predicting both time dependence and yields. For practical reasons, we consider a small number of kinetic populations, usually three. Our formalism enables not only wavelength-specific absorption and emission predictions, but also highly specific consideration of non-linear effects.

2. *Overview*

Oxygen-evolving photosynthetic organisms can regulate the relative flow of excitation energy into Systems I and II, making best use of that energy when System II is closed [40]. The early idea that this spill-over occurs passively through a connecting set of antenna molecules has recently been challenged (see, e.g., Ref. 43). Under various conditions of light saturation, salt concentration and phosphorylation, which have been found to control 'System-II–System-I transfer', freeze-fracture electron-microscope studies indicated actual physical movement of antenna chlorophylls from the region of System II to that of System I at physiological temperatures (see, for example, Refs. 44–46): thus, in a real sense the cross-sections for absorption are modified, not the energy-transferring mechanism. These results have created serious problems for the traditional interpretation of the

relationship between the 685 and 735 nm fluorescence time-courses. The newer picture is not without challenges, however; Haworth and Melis [46] have presented evidence that System I absorption cross-sections do not change under phosphorylation.

We have chosen to analyze the present data on considerably revised models mainly because of the new energy distribution viewpoint. Fig. 8c shows the underlying scheme adopted tentatively in this paper. Systems I and II are kinetically distinct. Part of the light-harvesting chlorophyll feeds population I′ (the antenna chlorophyll of System I) and part feeds population II. Population I′ feeds the emitters of F_{735}, C-705. It is assumed that all the fluorescences of LHC, I′, and II are included in the 685 nm data, while only that of C-705 is included in the 735 nm data. Essentially the rate constants k and K are adjusted to provide the biphasic rise at 735 nm, while K' and other decay constants and annihilation rates provide the decay phase of F_{685}.

While some F_{695} emission [47] is present in our F_{685} measurements, we have not conclusively associated it with one of the kinetic populations in our F_{685} analysis. Because of overlapping emission around F_{695} [35], its time-resolved fluorescence is complex and difficult to interpret [17].

3. Kinetic fits to time-resolved data

3A. F_{685}. We first try a simple sum of three exponential terms. Such an analysis, unless done with close attention to the complete eigenvalue problem for three-component kinetics, can only describe three decoupled fluorescing populations as sketched in Fig. 9a. Table I and Fig. 9a show

TABLE I

PARAMETERS USED IN THE FITS TO INTENSITY-DEPENDENT FLUORESCENCE

See the Appendix for details. The generic symbols refer to the general schemes of Fig. 11 and Eqn. A-1, and are not to imply any particular connection between the 685 and 735 nm cases.

Parameters and units	Generic Symbols	Quantities			
		685 nm fluorescence			735 nm fluorescence Coupled (Fig. 11d)
		Independent (Fig. 11a)	Coupled (Fig. 11b)	Coupled (Fig. 11c) [a]	
Chromophore density (cm^{-3})	N_{10}	$8\cdot10^{19}$	$8\cdot10^{19}$	$8\cdot10^{19}$	$8\cdot10^{19}$
	N_{20}	$8\cdot10^{19}$	$6\cdot10^{19}$	$8\cdot10^{19}$	$8\cdot10^{19}$
	N_{30}	$8\cdot10^{19}$	$1.3\cdot10^{19}$	$1\cdot10^{18}$	$8\cdot10^{19}$
Lifetime (no coupling, no annihilation) (ps)	τ_1	50	75	75	1200
	τ_2	375	375	1200	75
	τ_3	1200	1200	10000	1500
Ground-state absorption cross-section (cm^2)	σ_1	$0.6\cdot10^{-17}$	$1.5\cdot10^{-17}$	$1.5\cdot10^{-17}$	$3\cdot10^{-17}$
	σ_2	$1.0\cdot10^{-17}$	$1.5\cdot10^{-18}$	$1.5\cdot10^{-17}$	$3\cdot10^{-17}$
	σ_3	$1.8\cdot10^{-18}$	$1.9\cdot10^{-17}$	0	$3\cdot10^{-18}$
Excitation annihilation rate ($cm^3\cdot s^{-1}$)	γ_1	0	0	0	$6\cdot10^{-9}$
	γ_2	$4\cdot10^{-9}$	$6\cdot10^{-9}$	$2.5\cdot10^{-9}$	$1.2\cdot10^{-8}$
	γ_3	0	0	0	$5\cdot10^{-11}$
Transfer rate at low intensity ($N_{i0}k_{ij}$ is the rate from j to i) (ps^{-1})	$N_{20}k_{21}$	0	$k'=75^{-1}$	$k'=63^{-1}$	$k=50^{-1}$
	$N_{30}k_{32}$	0	$K'=0$	$k_T=667^{-1}$	$K=16^{-1}$
	$N_{20}k_{23}$	0	0	$k''=1250^{-1}$	0
Parameters assumed zero in all models	k_{12}, k_{13}, k_{31}, all σ_1's, k'_{12}	0	0	0	0

[a] These parameters are highly tentative and produce only a qualitatively satisfactory intensity dependence.

our fitting parameters. The necessary nonlinearity implicit in our data is reproduced with only one nonlinear effect, namely, annihilation in population II. The parameter needed, $\gamma_2 = 4 \cdot 10^{-9}$ cm$^3 \cdot$ s^{-1}, is typical of those introduced by various

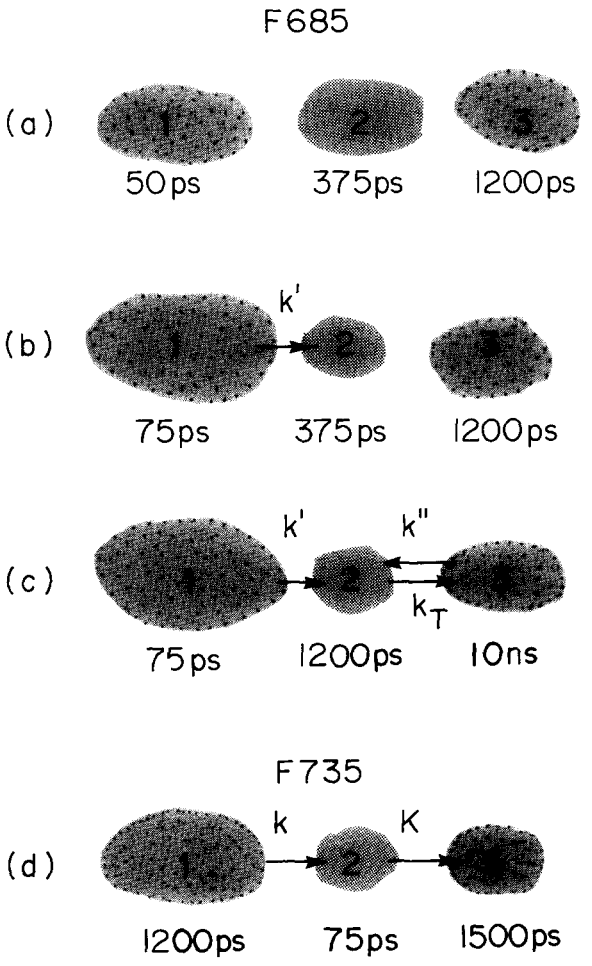

Fig. 9. Models for the basis of fluorescence emission. Fluorescence is contributed by each population with a time noted except for pool 3 in (c), which is explicitly a trap. (a) Independent population model, in which annihilation occurs in component 2. (b) Proximal antenna annihilation model, in which component 2 received excitation by transfer from component 1, and is again the only component in which annihilation takes place. The times given are the assumed lifetimes of the components in the absence of annihilation and trapping. (c) Similar to (b), except that a long-time component is simulated in population 2 by back-transfer from population 3. (d) Similar to (c), used for 735 nm case. Whereas in (a) these times are merely parameters, an attempt is made in the text to explain the values in (b).

authors to understand yield data [1]. The choice of γ_2 is quite critical and must be kept within 20% for a given set of other fixed parameters. As in all cases below, the parameters for this model were found by integrating the differential equations and adjusting the parameters according to a combination or our qualitative judgments as to fit and as to reasonableness on model grounds. The fits obtained were comparable to those shown in Fig. 4 which use the model described in Fig. 9b and Table I. Excitation was simulated accurately by a gaussian with a full width at half-maximum of 30 ps.

We make no interpretation of the numbers obtained on this independent population model, but note that the lifetimes are consistent with those found elsewhere in different contexts (see Fig. 1) and with those known for certain isolated chloroplast components. One criticism of this approach is that it provides no information on the most important feature of the organization of the light-harvesting antenna proteins and photosystems, that of being a coupled energy-transfer network.

A somewhat more interesting situation surrounds the fit on a model, Fig. 9b, which we call the proximal antenna annihilation model. Since the light-harvesting chlorophylls (LHC) emit at 680 nm [33–35,48], leaving the bulk of F_{685} to originate in Photosystem II antenna, annihilation is taking place in close competition with trapping. That is, rapid diffusion of excitation out of the LHC pool leads to a minimum of annihilation in the bulk but when the excitations have been funneled to the vicinity of the reaction center, their density is higher and annihilation is important. We have been able to reproduce our time-dependent results with a sum of three components described by model 9b and the parameters in Table I. Component 2 is the proximal antenna, which we simulated by keeping a normal density but lowering the molecular cross section for absorption. This means that annihilation processes can attain normal rates in this component, but the excitation must come generally from population 1. As suggested by the independent model, a population with very short life-times exists. We could not find a good fit with $\tau_1 = 1/k' > 100$ ps, and because we chose $1/k' =$ 75 ps the calculated overall lifetime of component 1 is really 37.5 ps in this model. The fits are shown

as smooth heavy curves in Fig. 4.

Chlorophyll densities were taken initially as $8 \cdot 10^{19}$ cm^{-3} (see, for example, Ref. 49) and the cross-sections close to those of chlorophyll *a* at 532 nm (see, for example, Ref. 31). The resultant weighted cross-sections are very close to the observed value in vivo [50]. The 375 ps lifetime of the annihilating pool is consistent with a room-temperature value of 400 ps $\pm$ 100 ps obtained independently by dual-pulse methods at room temperature [51].

The 75 ps intrinsic lifetime require for component 1 is unusual, but it will probably be clarified in a scheme which simultaneously handles both emission components.

The third component, life time 1200 ps, may represent fairly poorly connected chromophores, back-transfer from traps to the emitting pool (Fig. 9c), or a conbination of these. It is not immediately evident in our data on superficial inspection, because of our relatively short measurement duration. Nonetheless, we need the third component for the fit and not merely to link with other studies at longer times. An attempt to fit the data using the model of Fig. 9c was not too successful, but the best-fit parameters are shown in Table I. This model might be interpreted as the F_{695} component of our F_{685} being the third, long-lived component. Consider that F_{695} has been associated with System-II photochemistry [46], and a long lifetime component has been associated with F_{695} [35] and with back-transfer [17].

3B. F_{735}. The biphasic rise of F_{735} suggests the model of Fig. 9d, in which a 'nearby' pool of excitations first flows into the fluorescing species at a high rate K. After this pool's initial population is transferred, the 'distant' pool supplies excitation at a limiting rate k. We are assuming that only the third component contributes to fluorescence at 735 nm.

Fig. 5 shows our theoretical fits using the parameters in the last column of Table I as smooth heavy curves. As the excitation intensity increases, annihilation in the distant pool reduces the excitation available for transfer to the nearby pool, and ultimately that is the only one contributing to the fluorescent component. This does not occur for F_{685} because of the rapid transfer from the distant to the proximal pool.

Since we used a 30 nm filter at 735 nm, spectral inhomogeneity in emitters [33–36] may be causing the difficulty we found in getting good intermediate-intensity fits.

4. Intensity dependence of fluorescence yield

Using the simple method described in the Appendix, we have computed the fluorescence yield as a function of incident excitation intensity for the kinetic parameters shown in Table I including corrections for excited-state absorption. We have also integrated our fluorescence curves and have made absolute determinations of the total emission relative to that at low intensity. When a reasonable amount of excited-state absorption is included, which we take to be (1–3)-times the ground state cross-section [31], and transfer-rate saturation is defeated by the term k'_{ij} (see Appendix), the theoretical yield predictions at high intensities change considerably but the predicted time dependences do not. This shows that these additional nonlinearities, particularly excited-state cross-sections, are technically important but unfortunately have the main effect of obfuscating the interpretation of yield measurements.

Because the certain unresolved problems with fluorescence yield fitting which are, nonetheless, resolvable in principle, we regard our kinetics fits as preliminary, particularly the specifics of the long-time component. We are confident that a full explanation of the yields as well as time-courses will lead to a picture not unlike the present one, although somewhat different in numerical detail.

Summary

We have presented time-resolved data on the pulse-excited fluorescence of spinach chloroplasts at 685 and 735 nm, which bridge the gap between the linear, low-intensity limit in which photon counting is used and the very nonlinear high-intensity limit in which streak camera data with a lower signal-to-noise ratio have been previously available. We have demonstrated explicit agreement with the low-intensity results and have clarified the nature of the rising phase of the 735 nm fluorescence. We have also shown the feasibility of matching the data with the results of directly integrating model kinetic equations, a process

which reverses the usual analysis: deconvolution is replaced by convolution and the the use of arbitrary fitting parameters is replaced by true kinetic modelling. The proximal antenna annihilation model is fairly successful in describing 685 nm fluorescence data versus intensity. While more supporting evidence is needed to justify this scheme, it incorporates an important idea, namely that there is rapid transfer from the LHC pool to another pool in which the majority of the annihilation processes occur. Although the relatively large number of parameters in our procedure precludes simple optimization, the directness of the approach compensates for the absence of assurance that unique set or the 'best' set of parameters has been found. What we have found are sets that work and are physically reasonable. It is important to reemphasize that one and only one set of equations explains the data without changing any parameters as the excitation intensity passes into the nonlinear region.

Acknowledgements

This research was supported in part by the National Science Foundation under grants PCM-80-11819, PCM-83-03004 (operations) and PCM-80-18488 (Subpicosecond Biological Physics Facility), in part by the United States Department of Agriculture under grant 82-CRCR-1-1128, and in part by the sponsors of the Laser Fusion Feasibility Project of the University of Rochester. The contribution of N.E.G. and J.B. to this work was in part supported by National Science Foundation Grant PCM-83-08190 at New York University. One of the authors (R.S.K.) acknowledges the support and interest of the Aspen Center for Physics where part of the theoretical work was done in July 1982. The authors wish to thank G.A. Mourou and G. Paillotin for helpful discussions and technical advice. They also appreciate the valuable assistance of C.A. Hanzlik with sample preparations and data plotting and D. Dutkevitch with programming.

Appendix. Three-component kinetics with nonlinear terms

The three-component formalism used in the Analysis section and illustrated in Fig. 10 is based on the following set of equations:

$$\frac{dN_1(t)}{dt} = [N_{10} - N_1(t)][\sigma_1 I(t) + k_{12}N_2(t) + k_{13}N_3(t)] - N_1(t)\left\{\frac{1}{\tau_1} + [N_{20} - N_2(t)]k_{21} + [N_{30} - N_3(t)]k_{31} + \gamma_1 N_1(t) + \sigma_1' I(t)\right\} \quad \text{(A-1)}$$

$$\frac{dN_2(t)}{dt} = \left(\begin{array}{l}\text{same as for } N_1 \text{ with cyclic} \\ \text{permutation of labels } 1 \to 2 \to 3 \to 1\end{array}\right) - k'_{12}N_1(t)N_2(t) \quad \text{(A-2)}$$

$$\frac{dN_3(t)}{dt} = \left(\begin{array}{l}\text{same as for } N_1 \text{ with cyclic} \\ \text{permutation of labels } 1 \to 3 \to 2 \to 1\end{array}\right) \quad \text{(A-3)}$$

The factor $N_{10} - N_1(t)$ is the number (or number density) of ground-state molecules of type 1 if N_{10} is the total number and $N_1(t)$ the number of excited molecules of type 1. Therefore, if $N_1(t)$ is the number of molecules of type 1 in the first-excited singlet state, this factor is approximately the number of ground-state molecules of type 1. If they have an absorption cross-section σ_1 (in cm^2) and there is an intensity $I(t)$ (in photons per cm^{-2} per s), and if the absorption process leads to production of first-excited-state molecules, then the term $[N_{10} - N_1(t)]\sigma_1 I(t)$ acts as the primary source term for the quantity $N_1(t)$. Stimulated

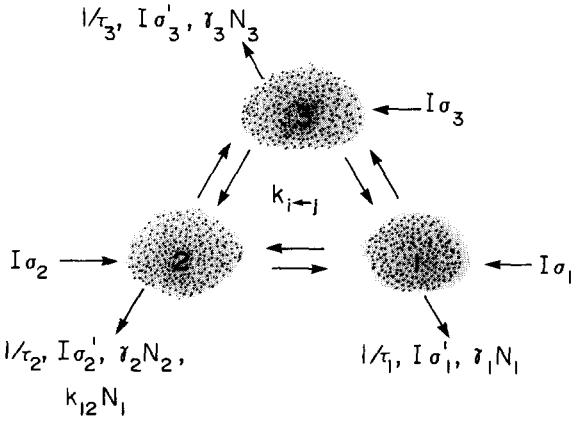

Fig. 10. The kinetic scheme of the equations discussed in the appendix is totally symmetric under permutations (123) except that population 2 may have the extra loss term k'_{12} (see text).

emission is not included here, as we consider broad-band systems in which the excitation light is not in resonance with the emitted light.

The second term, $[N_{10} - N_1(t)]k_{12}N_2(t)$, provides transfer from population 2 to population 1, and k_{12} is a bimolecular rate in the usual sense (in $cm^3 \cdot s^{-1}$ if the N_{i0} are number densities). If there are fewer groundstate molecules of type 1, there must be less transfer which produces 'N_1's'. In simpler kinetic schemes the nonlinear aspect of such a transfer rate is ignored and $N_{10}k_{12}$ is a simple rate called w_{12} or F_{12}. Similar remarks hold for the k_{13} term, and for the k_{21} and k_{31} terms by which the N_1 population loses to the others.

The remaining loss terms are straightforward: N_1/τ_1 is the rate of loss of population 1 by monomolecular processes (fluorescence, radiationless decay and intersystem crossing). Incidentally, although one of the populations here could easily represent triplets, the equations were developed for picosecond processes in which triplet buildup is negligible. The term $\gamma_1 N_1(t)^2$ represents annihilation and $\sigma_1' I(t)N_1(t)$ the net loss of population 1 through excited-state absorption.

An extra loss term $k_{12}' N_2(t)N_1(t)$ has been included for a particular application in which transfer from population 2 to population 1 proceeds despite the depletion of the number of ground-state molecules in population 1. Five more similar 'interpopulation annihilation' terms could be included.

Eqns. (A-1)–(A-3) have been solved by numerical integration, using either the actual pulse shape for $I(t)$ or a Gaussian when appropriate. The results may then be integrated to obtain the number of quanta emitted by species 'i':

$$N_i \equiv (\phi_{i0}/\tau_i) \int_{t=0}^{\infty} N_i(t)\mathrm{d}t$$

and the total number of quanta absorbed by both the ground and excited states of species 'i':

$$D_i = \int_{t=0}^{\infty} I(t)[\sigma_i(N_{i0} - N_i) + \sigma_i' N_i]\mathrm{d}t$$

Here ϕ_{i0} is the normal quantum yield of species 'i' alone $\phi_{i0} = \tau_i/\tau_{i0}$, where τ_{i0} is its natural radiative lifetime. The yields:

$$\phi_i = \frac{N_i}{D_1 + D_2 + D_3}$$

are then proportional to measured quantum yields of fluorescence where the model applies and they satisfy the restriction:

$$\sum_i \phi_i \leqslant 1$$

References

1 Breton, J. and Geacintov, N.E. (1980) Biochim. Biophys. Acta 594, 1–32
2 Breton, J. and Roux, E. (1975) in Lasers in Physical Chemistry and Biophysics (Joussot-Dubien, J., ed.), pp. 379–388, Elsevier/North-Holland, Amsterdam
3 Beddard, G.S., Porter, G., Tredwell, C.J., and Barber, J. (1975) Nature 258, 166–168
4 Campillo, A.J., Kollman, V.H. and Shapiro, S.L. (1976) Science 193, 227–229
5 Breton, J. and Geacintov, N.E. (1976) FEBS Lett. 69, 86–89
6 Paillotin, G., Swenberg, C.E., Breton, J., and Geacintov, N.E. (1979) Biophys. J. 25, 513–534
7 Geacintov, N.E., Swenberg, C.E., Campillo, A.J., Hyer, R.C., Shapiro, S.L. and Winn, K.R. (1978) Biophys. J. 24, 347–359
8 Magde, D., Berens, S.J., and Butler, W.L. (1982) in Picosecond Lasers and Applications, Proceedings of SPIE – The International Society for Optical Engineering (Goldberg, L.S., ed.), Vol. 322, pp. 80–86, SPIE, Bellingham, WA
9 Gulotty, R.J., Fleming, G.R. and Alberte, R.S. (1982) Biochim. Biophys. Acta 682, 322–331
10 Nairn, J.A., Haehnel, W., Reisberg, P., and Sauer, K. (1982) Biochim. Biophys. Acta 682, 420–429
11 Searle, G.F.W., Tredwell, C.J., Barber, J. and Porter, G. (1979) Bichim. Biophys. Acta 545, 496–507
12 Beddard, G.S., Fleming, G.R., Porter, G., Searle, G.F.W. and Synowiec, J.A. (1979) Biochim. Biophys. Acta 545, 165–174
13 Campillo, A.J., Shapiro, S.L., Geacintov, N.E. and Swenberg, C.E. (1977) FEBS Lett. 83, 316–320
14 Pellegrino, F., Dagen, A., Sekuler, P. and Alfano, R. (1983) Photobiochem. Photobiophys. 6, 15–23
15 Sauer, K. and Brewington, G.T. (1977) in Proceedings of the 4th International Congress on Photosynthesis (Hall, D.O., Coombs, J. and Goodwin, T.W., eds.), pp. 409–421, Biochemical Society, London
16 Yu, W., Pellegrino, F. and Alfano, R.R. (1977) Biochim. Biophys. Acta 460, 171–181
17 Reisberg, P., Nairn, J.A. and Sauer, K. (1982) Photochem. Photobiol. 36, 657–661
18 Lavorel, J., and Etienne, A.-L. in Topics in Photosynthesis (Barber, J., ed.), Vol. 2, Chap. 6, esp. pp. 218–219, Elsevier, Amsterdam

19 Satoh, K. and Butler, W.L. (1978) Biochim. Biophys. Acta 502, 103–110
20 Geacintov, N.E., Breton, J., Swenberg, C.E., Campillo, A.J., Hyer, R.C. and Shapiro, S.L. (1977) Biochim. Biophys. Acta 461, 306–312
21 Breton, J., Roux, E. and Whitmarsh, J. (1975) Biochem. Biophys. Res. Commun. 64, 1274–1277
22 Seka, W. and Bunkenburg, W. (1978) J. Appl. Phys. 49, 2277–2280
23 Paillotin, G., Geacintov, N.E. and Breton, J. (1983) Photochem. Photobiol. 37, 475–478
24 Knox, W. and Mourou, G. (1981) Opt. Commun. 37, 203–206
25 Knox, W. and Forsley, L. (1983) ACS Symposium Series 236, 221–231
26 Knox, W. (1983) Ph.D. thesis, University of Rochester
27 Haehnel, W., Nairn, J.A., Reisberg, P. and Sauer, K. (1982) Biochim. Biophys. Acta 680, 161–173
28 Kepler, R.G., Caris, J.C., Avakian, P. and Abramson, E. (1963) Phys. Rev. Lett. 10, 400–402
29 Swenberg, C.E., Geacintov, N.E. and Pope, M. (1976) Biophys. J. 16, 1447–1452
30 Geacintov, N.E. Breton, J., Swenberg, C.E. and Paillotin, G. (1977) Photochem. Photobiol. 26, 629–638
31 Shepanski, J.F. and Anderson, R.W. (1981) Chem. Phys. Lett. 78, 165–173
32 Butler, W.L., Tredwell, C.J., Malkin, R. and Barber, J. (1979) Biochim. Biophys. Acta 545, 309–315
33 Garab, G.I. and Breton, J. (1976) 71, 1095–1102
34 Moya, I. (1970) Ph.D. thesis, Université de Paris Sud
35 Moya, I., Mullet, J.E., Briantais, J.-M. and Garcia, R. (1981) Proceedings of the 5th International Congress on Photosynthesis, (Akoyunoglou, G., ed.), pp. 163–172, Balaban International Science Services, Philadelphia, PA
36 Kramer, H.J.M. and Amesz, J. (1982) Biochim. Biophys. Acta 682, 201–207
37 Murata, N., Nishimuro, N. and Takamiya, A. (1966) Biochim. Biophys. Acta 126, 234–243
38 Shipman, L.L. (1980) Photochem. Photobiol. 31, 157–167
39 Mauzerall, D. (1976) Biophys. J. 16, 87–91
40 Paillotin, J., Geacintov, N.E. and Breton, J. (1983) Biophys. J. 44, 65–77
41 Den Hollander, W.T.F., Bakker, J.G.C. and Van Grondelle, R. (1983) Biochim. Biophys. Acta 725, 492–507
42 Bonaventura, C. and Myers, J. (1969) Biochim. Biophys. Acta 189, 366–383
43 Barber, J. (1983) Photobiochem. Photobiophys. 5, 181–190
44 Anderson, J.M. (1981) FEBS Lett. 124, 1–10
45 Kyle, D.J., Haworth, P. and Arntzen, C.J. (1982) Biochim. Biophys. Acta 680, 336–342
46 Haworth, P. and Melis, A. (1983) FEBS Lett. 60, 277–280
47 Breton, J. (1982) FEBS Lett. 147, 16–20
48 Rijgersberg, C.P. (1980) Ph.D. thesis, University of Leiden
49 Knox, R.S., and Davidovich, M.A. (1978) Biophys. J. 24, 689–712
50 Geacintov, N.E., and Breton, J. (1982) in Trends in Photobiology, Proceedings of the 8th International Congress on Photobiology (Helene, C., Charlier, M., Montenay-Garestier, Th. and Laustriat, G., eds.), pp. 549–559, Plenum, New York
51 Dobek, A., Deprez, J., Geacintov, N.E., Paillotin, G. and Breton J. (1984) Biochim. Biophys. Acta 806, 81–92